

Supplement of Atmos. Chem. Phys., 16, 3099–3126, 2016
<http://www.atmos-chem-phys.net/16/3099/2016/>
doi:10.5194/acp-16-3099-2016-supplement
© Author(s) 2016. CC Attribution 3.0 License.



Atmospheric
Chemistry
and Physics
Open Access
EGU

Supplement of

Atmospheric methane evolution the last 40 years

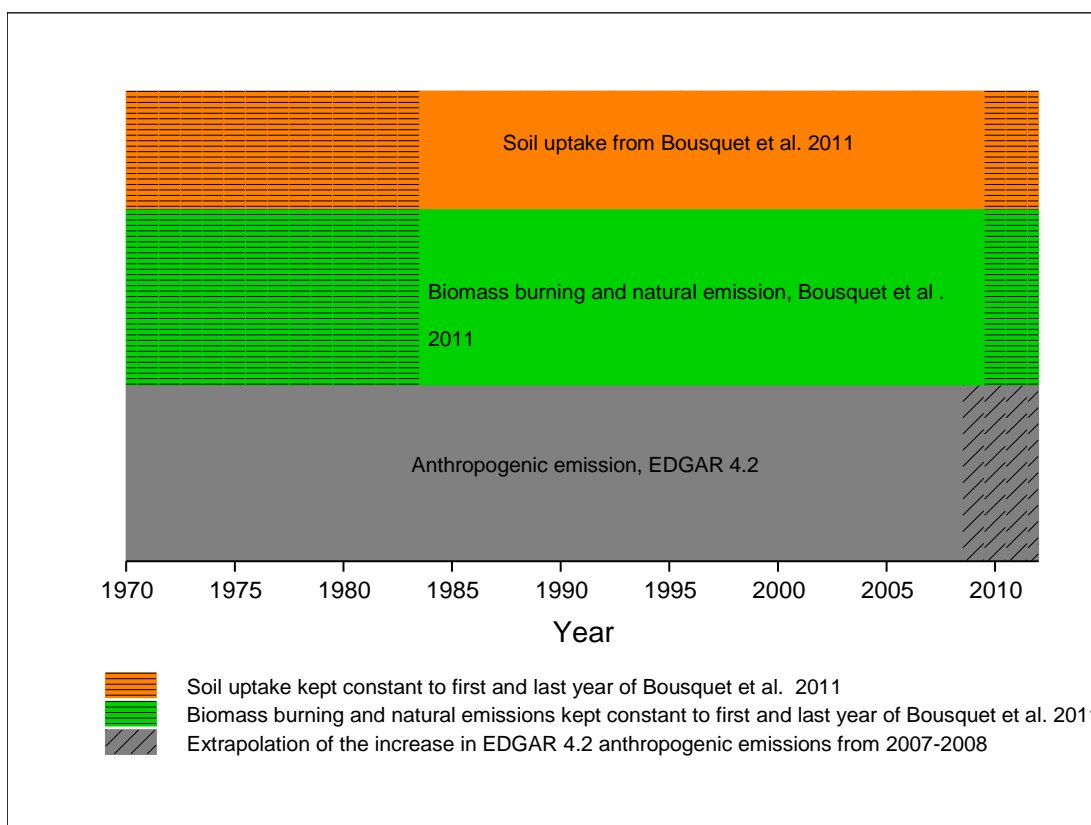
Stig B. Dalsøren et al.

Correspondence to: Stig B. Dalsøren (stigbd@cicero.oslo.no)

The copyright of individual parts of the supplement might differ from the CC-BY 3.0 licence.

1 **S1 Setup of emission inventories in model simulations**

2



3

4 **Figure S1.** Overview of how emission inventories are included in the model for different time
5 periods.

6

7 **S2 Emission sectors and tracers**

8 **Table S1.** List of CH₄ emission sectors and emission tracers used in the model simulations.

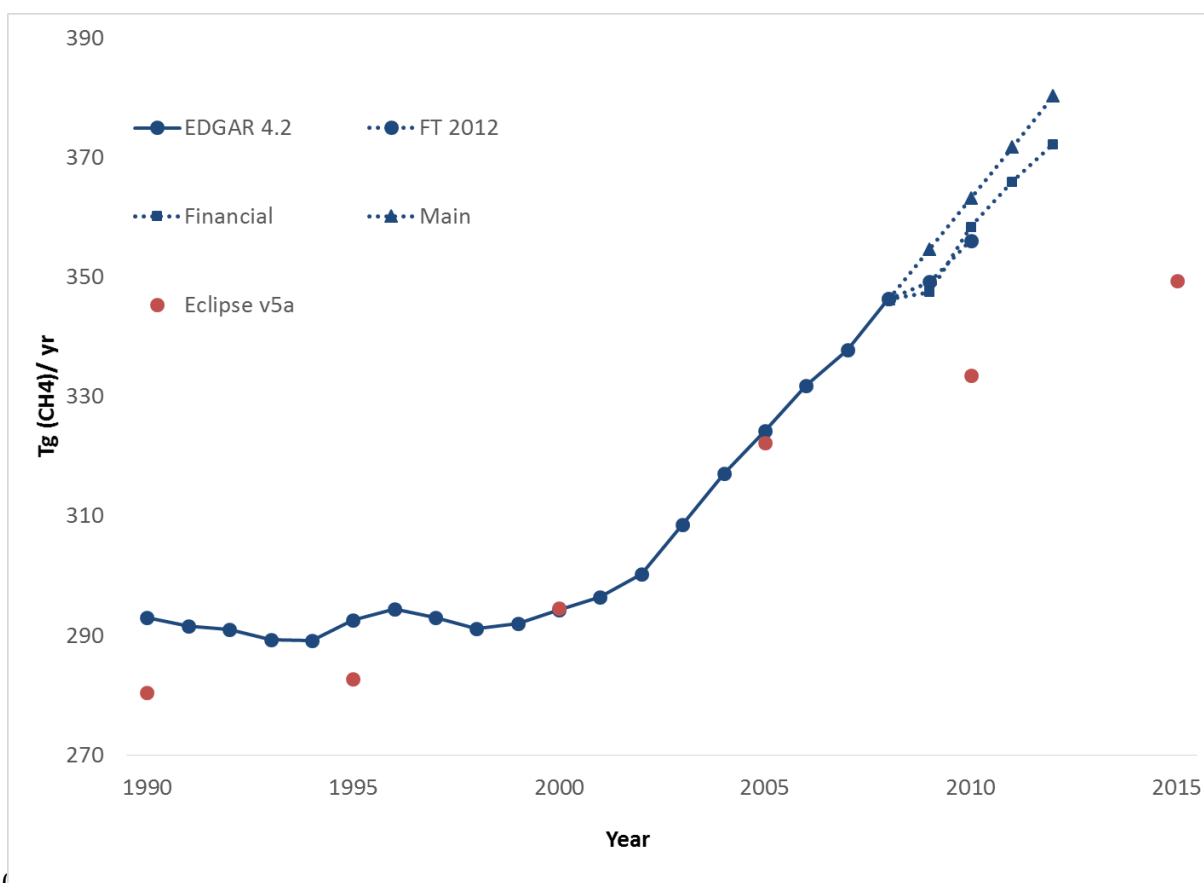
9 The text colours in column 1 and 2 shows the legend colours in Fig. 1 and Fig. 6-10.

Wetlands	Emissions shown in Fig. 1	Tracer from these sectors shown in Fig. 6-10, 12-14, named "Natural"
Biomass burning	Emissions shown in Fig. 1	
Oceans+Termites+other natural	Emissions shown in Fig. 1	
Enteric fermentation	Emissions shown in Fig. 1	Tracer from this sector shown in Fig. 6-10, 12-14
Agricultural soils	Emissions shown in Fig. 1	Tracer from this sector shown in Fig. 6-10, 12-14
Solid fuels: Fugitive from solids	Emissions shown in Fig. 1	Tracer from this sector shown in Fig. 6-10, 12-14
Gas production and distribution	Emissions shown in Fig. 1	Tracer from this sector shown in Fig. 6-10, 12-14
Sum all other anthropogenic (those listed below)	Emissions shown in Fig. 1	Tracer from this sector shown in Fig. 6-10, 12-14
Solid waste		
Waste water		
Residential		
Manure management		
Energy manufacturing transformation		

Agricultural waste burning		
Road transportation		
Fossil fuel fires		
Non-road transportation		
Oil production and refineries		
Industrial process and product use		

1
2 The EDGAR v4.2 inventory was recently extended with the years 2009-2012. In this update
3 abbreviated FT 2012 a somewhat simplified (Fast Track) approach was used and other
4 emission components (NO_x, CO, NMVOCs) have not been updated yet. In Fig. S2 we
5 compare our extrapolations after 2008 with the new data. We also compare the EDGAR
6 inventory to the ECLIPSE v5a emission inventory that are available for part of our study
7 period (1990-2015), on 5-year intervals:

8 <http://www.iiasa.ac.at/web/home/research/researchPrograms/ECLIPSEv5.html>).
9



10
11
12 **Figure S2.** Comparison of emission inventories. The EDGAR v4.2 extended with the
13 EDGAR FT2012 update compared to the extrapolations (main, financial) we made due to

1 missing data at the start-up of this study. A comparison to the ECLIPSE v5a inventory is also
2 shown.

3
4 The EDGAR FT 2012 curve in Fig. S2 ends in 2010 since it is not possible to exclude
5 biomass burning for the numbers available for 2011 and 2012. From the figure it is evident
6 that our simple baseline extrapolation (main) likely overestimates the emissions after 2008
7 and that the approach trying to take into account the financial crisis is closer to reality. In that
8 approach BP statistics for gas production, oil and coal consumption were used to scale
9 relevant methane emission from oil, gas and coal production. If this approach were to be used
10 to set up a consistent baseline emission inventory, these BP factors should also be used to
11 scale emissions of other compounds (e.g. CO and NO_x). This would be more complicated and
12 introduce uncertainties as it is less clear how to use the BP factors to scale emissions for road
13 traffic, power plants etc., which constitute a substantial share of the emissions for these
14 compounds. Therefore, a simpler extrapolation based on changes for previous years was
15 preferred as baseline since it can be used in a consistent way for all emitted compounds.

16
17 The total emissions in the EDGAR and ECLIPSE inventories are rather similar but there
18 are large differences in temporal evolution. ECLIPSE has larger emission growth from
19 1995 to 2000 and much smaller growth from 2005-2010. In the main text we explain why
20 we think the time evolution in the ECLIPSE inventory is more realistic. The step from
21 2010 to 2015 in ECLIPSE is scenario based but should give some direction on where
22 current emission levels are.

23 24 **S3 Theoretical foundation of the use of the fictitious tracers**

25 As indicated in Sect. 2.2 of the main paper, the simulations used 18 passive fictitious tracers
26 for each of the CH₄ emission sectors listed in Table S1. The tracers were continuously emitted
27 and then given an e-folding lifetime of 1 month undergoing transport but not interacting
28 chemically. These tracers were used as a proxy for the different sector's recent contribution to
29 monthly mean surface CH₄ concentrations, with the aim of revealing key sectors and regions
30 behind recent changes in spatial distribution or temporal evolution of CH₄. In this section, we
31 provide the theoretical foundation that justifies the use of these fictitious tracers.

32
33 Firstly, we summarize the results obtained in this section. We split the CH₄ mole fraction into
34 two components: a quite uniform background component (r_B) and an inhomogeneous recently

1 emitted component (r_R); the fictitious tracer being a proxy for the second component. The
 2 CH_4 surface emissions act as the sources for r_R (not for r_B), then this component is advected
 3 and mixed, and when achieving a good mixing (after 1-2 months) it is converted into r_B . Since
 4 the life time of r_R is of around 1 month (much smaller than the mean CH_4 lifetime), the
 5 chemical destruction acting on r_R is almost negligible (only acts on r_B). The same reason
 6 makes $|r_B| \gg |r_R|$, except very near strong CH_4 emission sources.

7
 8 We start with the continuity equation for the CH_4 mole fraction (r) in dry air:

$$9 \quad \frac{Dr}{Dt} = -\frac{1}{n} \nabla \cdot \bar{F}_D(r) - \sum_i k_i \cdot c_i \cdot r \quad (1),$$

10 where D/Dt is the Lagrangian time derivative, n is the number density (mol/m^3) of the dry air,
 11 the vector F_D is the diffusive flux due to turbulence (i.e., unresolved flow by the spatial scale
 12 of the model), k_i is the reaction rate with the trace gas i and c_i is the number density of the
 13 trace gas i . Note that the diffusive flux is linear in r (e.g., proportional to the gradient of r),
 14 even in the case in which the flux is non local (e.g., see Holtslag & Boville, 1993), as well as
 15 the rest of the terms of Eq. (1). The surface sources and sinks enter as the boundary conditions
 16 of Equation (1).

17
 18 Now, we split Eq. (1) into two equations (this is our definition for the components r_B and r_R ;
 19 we do not base our definition in spatial averages):

$$20 \quad \frac{Dr_B}{Dt} = -\frac{1}{n} \nabla \cdot \bar{F}_D(r_B) - \sum_i k_i \cdot c_i \cdot r_B + P(r_R) \quad (2),$$

$$21 \quad \frac{Dr_R}{Dt} = -\frac{1}{n} \nabla \cdot \bar{F}_D(r_R) - \sum_i k_i \cdot c_i \cdot r_R - P(r_R) \quad (3),$$

22 where the chemical losses in Eq. (3) will be almost negligible except very near strong CH_4
 23 sources (as explained in the second paragraph of this section), and P is a linear projector onto
 24 a complete set of vectors (spectral components) for wavelengths larger than around 6,000 km.
 25 This projector continuously removes the smoothed part of r_R , which is continuously created as
 26 the emitted CH_4 becomes well mixed, and converts it into r_B . The CH_4 surface emissions are
 27 only included as boundary conditions for Eq. (3) (not for Eq. (2)). The CH_4 surface sink is
 28 only included as boundary condition for Eq. (2). Note that summing Eqs. (2) and (3), Eq. (1)
 29 is obtained. The reason for chosen 6,000 km as threshold wavelength is: 1) The mid-latitude
 30 synoptic scale motions have a characteristic variation length, L , of around 1,000 km (e.g., see
 31 Holton, 1992), and their associated wavelength is therefore of around 6,000 km. 2) Synoptic

1 scale latitudinal motions are able to build up mole fraction inhomogeneities by advection of
 2 the CH₄ climatological latitudinal pattern. 3) What makes more sense is to convert r_R into r_B
 3 around the smaller scale in which the background by itself can build up inhomogeneities.
 4 Anyway, in the main article we plot and analyse monthly averages, therefore the mole
 5 fraction mark due to synoptic motions will be smoothed.

6
 7 In the main paper, instead of using the non-local projector operator for coupling r_R and r_B , we
 8 use a simpler local proxy for this purpose: a volumetric sink for r_R with an e-folding lifetime
 9 of 1 month ($A \times r_R$ instead of $P(r_R)$, with $A=1 \text{ month}^{-1}$). This process can approximately
 10 mimic the projector behaviour: it transforms r_R into r_B at a rate similar to that in which the
 11 projector acts (i.e., the rate at which mixing is able to smooth the emitted CH₄ till the 1,000
 12 km characteristic variation length at which the projector starts to act). Indeed, r_R will be
 13 underestimated a bit because part of it will be removed by the 1-month lifetime e-folding sink
 14 before being smoothed to the 1,000 km characteristic variation length. The time needed to
 15 mix a species throughout a hemisphere is about 1 to 2 months, whereas 1 to 2 years are
 16 needed to mix a species through the entire Earth troposphere (Seinfeld and Pandis, 1998).

17
 18 Now, we introduce the following notation: (Eulerian) annual means are denoted as $\langle \rangle$ (in the
 19 main paper we use annual running means since we are interested in the inter-annual variation
 20 of CH₄), whereas longitudinal means along a whole terrestrial parallel are denoted as $[]$. Each
 21 variable can be decomposed in two components: the mean and the deviation from the average,
 22 for instance:

$$23 \quad r = \langle r \rangle + r' \quad (4)$$

$$24 \quad r = [r] + r^* \quad (5)$$

$$25 \quad \langle r \rangle = [\langle r \rangle] + \langle r \rangle^* \quad (6)$$

26 where ' denotes time fluctuations and * denotes longitudinal fluctuations.

27 We have found (see the main paper) that there is a high correlation between $\langle r \rangle^*$ and $\langle r_R \rangle^*$
 28 for most of the stations, with r_R defined using the local 1-month e-folding sink. Writing Eqs.
 29 (1) and (3) in conservative form, and expanding each variable simultaneously into its
 30 longitudinal and time components, in a similar fashion than Sect. 4.1.1 of Peixoto and Oort
 31 (1992), we have obtained quite complex PDEs (Partial differential Equations) linear in $\langle r \rangle^*$
 32 and $\langle r_R \rangle^*$, respectively. Both equations are very similar (it is out of the scope of this paper to
 33 present such equations), and the main differences are:

- 1 a) a term containing the flux $\langle r \rangle \langle v \rangle^*$ appears in the first equation, whereas $\langle r_R \rangle$
2 $\langle v \rangle^*$ appears in the second equation (they are no homogeneous terms of the
3 corresponding PDEs).
4 b) a chemical term containing $\langle k_i c_i \rangle^* \langle r_B \rangle$ appears in the first equation, whereas the
5 term $-A n \langle r_R \rangle^*$ appears in the second equation.

6 We expect these terms are usually small (because we expect $\langle v \rangle^*$ and $\langle k_i c_i \rangle^*$ are usually
7 small; these are the prerequisites mentioned in the main paper), except the term $-A n \langle r_R \rangle^*$
8 that we think it is compensated in the other PDE by a larger mixing (due to differential
9 advection and turbulent diffusion), which tends to convert $\langle r \rangle^*$ into $\langle r \rangle$. If both PDEs were
10 identical, there would be a linear relation between their solutions, and the time linear
11 correlation coefficient between the solutions would be exactly 1.

12 However, the few small differences between both PDEs make the time correlation coefficient
13 between the solutions smaller than one. Note that $\langle r \rangle^*$ changes along the corresponding
14 parallel. For locations with $|\langle r \rangle^*|$ small (i.e., $\langle r \rangle$ closes to $\langle r \rangle$) compared to the maximum
15 and minimum within the parallel, the relative contribution of the terms different (between the
16 PDEs) may be larger and therefore the correlation coefficient smaller for these locations (this
17 might explain the case of the Wendover station). As mentioned in the previous paragraph, r_R
18 will be underestimated a bit when using the 1-month e-folding sink term, and this fact can
19 contribute to the offset between $\langle r \rangle^*$ and $\langle r_R \rangle^*$, and might explain why for most of the
20 stations $|\langle r \rangle^*| > |\langle r_R \rangle^*|$.

23 **S4 Scaling procedure**

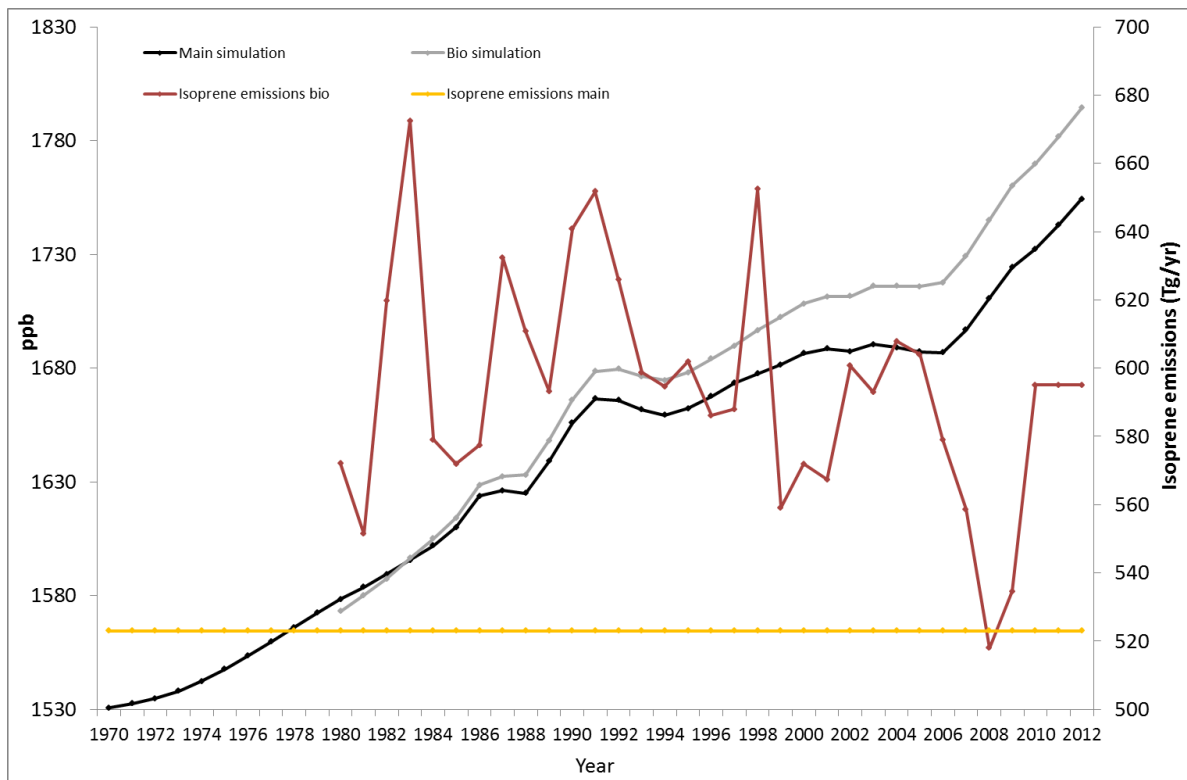
24 As noted in the main text the model in general underestimates the observed surface methane
25 levels and likely reasons are discussed there. In Fig. 6-10 in the main article, the model results
26 are scaled to the observed mean over the periods of measurements to better discern
27 differences in trends between observations and model. To do this the absolute difference
28 between the model output and the measurements is calculated for each year in the period
29 1970-2012. The mean of these differences is then added to the modelled values for all years.
30 The model values are sampled from the gridbox with the closest location to the geographical
31 position of the stations. Likewise, the model layer best corresponding to the station altitude is
32 used.

34 **S5 Discussion of sensitivity studies**

1 **S5.1 Influence of inter-annual variation in emissions from vegetation**

2 In the “main” simulation discussed in the main article, natural emission data for 2000 were
3 used for all years and all components except CH₄. The emissions from vegetation of CO and
4 NMVOCs are from MEGAN (Guenther et al., 2006). Recently a new dataset (Sindelarova et
5 al., 2014) with MEGAN emissions covering the period 1980-2010 became available. This
6 dataset was used in the “bio” simulation to investigate whether inter-annual variations in CO
7 and NMVOCs emissions from vegetation are important for the CH₄ evolution. Variations in
8 these emissions affect OH levels which in turn influence the atmospheric CH₄ loss. Fig. S3
9 shows that surface CH₄ levels are higher in the “bio” simulation. Due to the long response
10 time of CH₄ the difference between the two simulations grows over the first two decades. The
11 higher CH₄ level is expected since the emissions (illustrated by the isoprene emission curves
12 in Fig. S3) in the new inventory are higher for most years compared to the constant year 2000
13 emissions in the old inventory. Larger emissions of components like isoprene and CO results
14 in lower OH values and reduced CH₄ loss. However, accounting for inter-annual variation of
15 vegetation emissions of CO and NMVOCs does not shift the periods of growth and
16 stagnation. Neither does it lead to larger year to year fluctuations in CH₄ levels. Compared to
17 surface measurements (discussed in section 3.2 of the main article) the underestimation of
18 CH₄ levels is less in the “bio” simulation, except from that there is no improvement in model
19 performance.

20

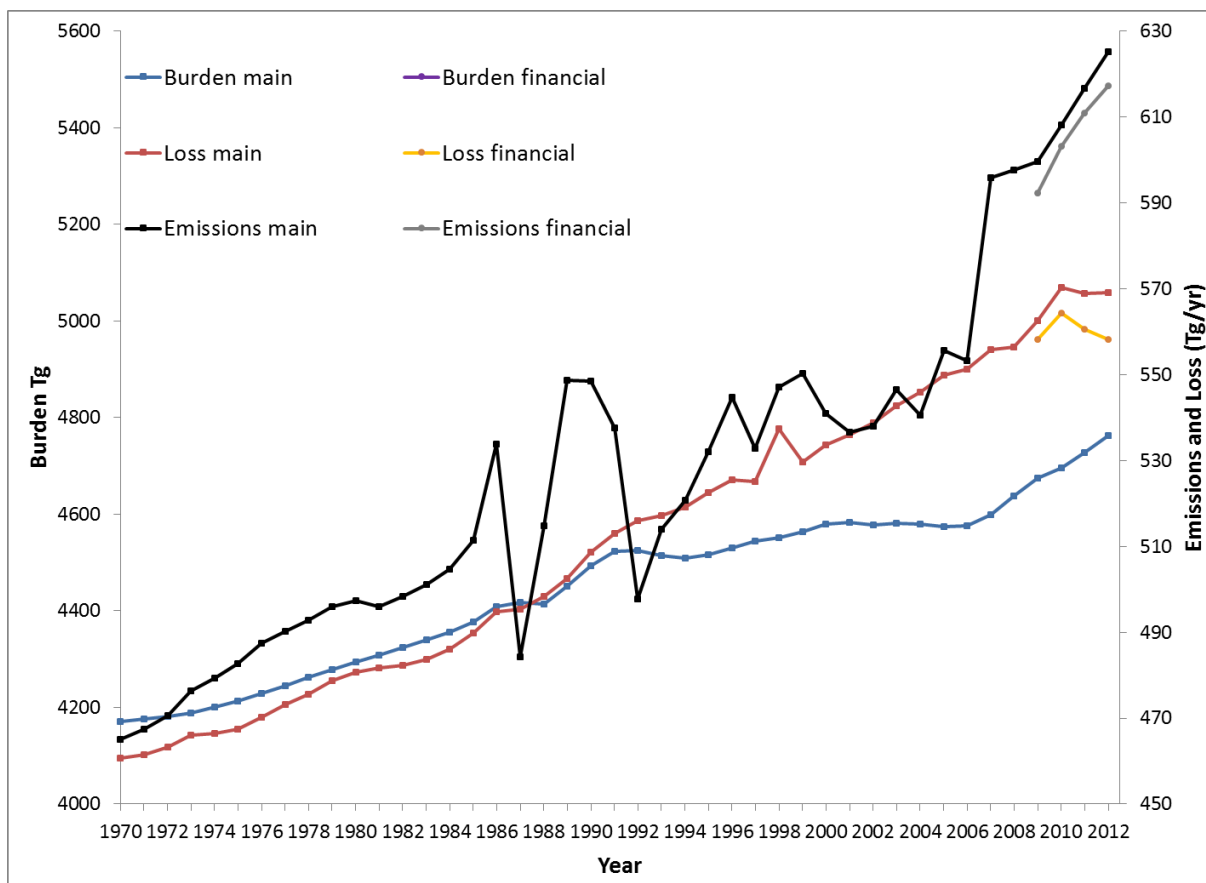


1
2 **Figure S3.** Surface CH₄ levels and isoprene emissions in main simulation and bio simulation.

3
4 **S5.2 Influence of financial crisis.**

5 The period 2009-2012 was rerun with slightly different emissions evaluating whether the
6 recent financial crisis had any significant impact on CH₄ levels. Here, the emissions from
7 petroleum and solid fuel production and distribution were scaled with BP Statistical Review
8 of World Energy (bp.com/statisticalreview) numbers for gas production, oil and coal
9 consumption resulting in a drop in total emissions in 2009 (Fig. 1, main article and Fig. S4).
10 However, the evolution in emissions from 2010 with this alternative extrapolation is rather
11 similar to that for the standard extrapolation. Due to the drop in emissions in 2009 in the
12 “financial” run methane loss after 2009 is lower than for the “main” simulation (Fig. S4). The
13 emission growth in 2011 and 2012 is also slightly lower in the financial simulation. This
14 results in declining methane loss for these years in the “financial” simulation. In contrast the
15 methane loss in 2011 and 2012 is rather stable in the “main” simulation. Despite differences
16 for the methane loss the methane burden is very similar in the two simulations. Therefore, it
17 seems likely that the financial crisis had small impact on the methane burden, but due to the
18 long methane lifetime some of the difference in methane loss could manifest as burden
19 changes after 2012, which is the end-year of our simulations.

20



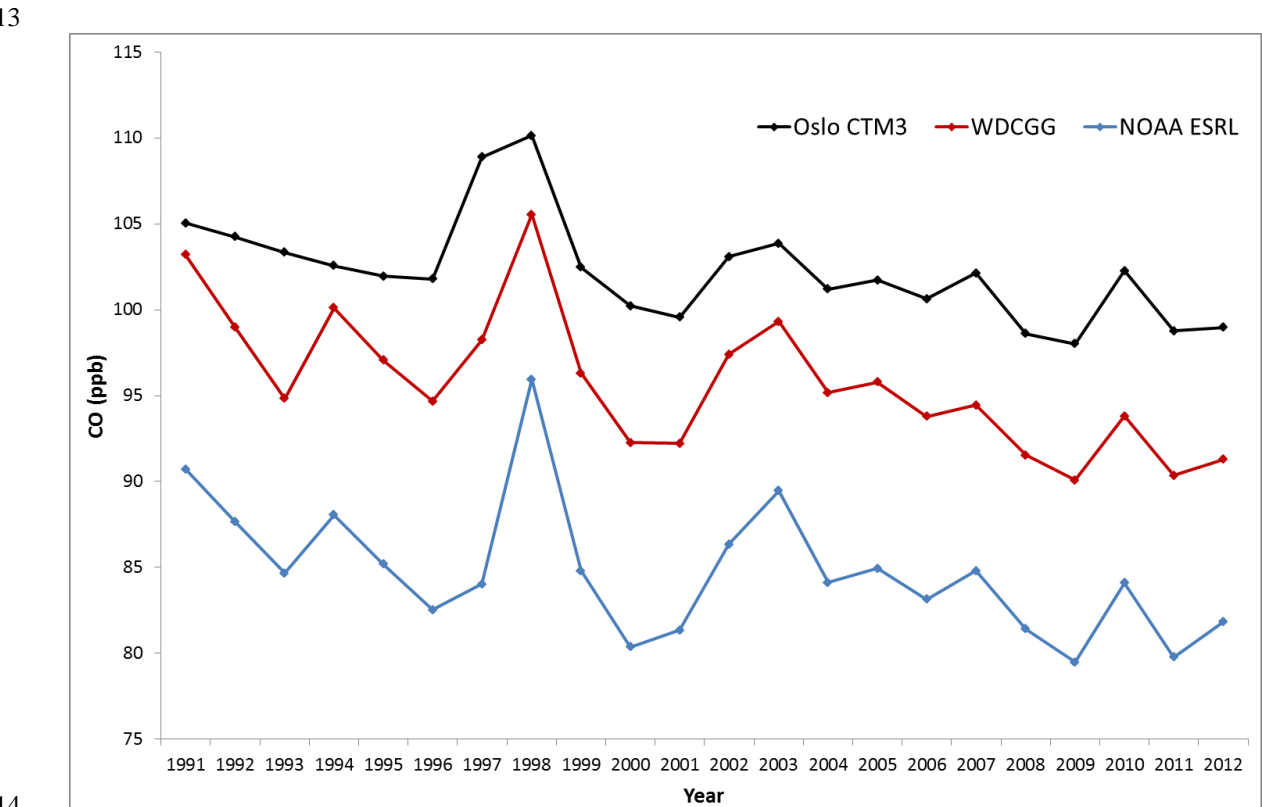
1
2 **Figure S4.** Methane budget in main and financial simulations.
3
4

5 **S6 Comparison with CO observations**

6
7 Since reaction with OH is the major loss of CO from the atmosphere a comparison with CO
8 measurements indicates whether modelled trends in CO and OH, and the applied CO emission
9 inventory are internally consistent.. In this section, a first elementary evaluation is made based
10 on comparison between our model results and observation-based estimates of global mean
11 surface CO levels (Fig. S5). There is very good agreement for the long term evolution (years-
12 decades). The same is the case for short term (year to year) variations, especially after 1996
13 when our simulations include inter-annual variability in meteorology and biomass burning
14 emissions (CO, NO_x and NMVOCs). Our simulations do not fully account for the effect of
15 the Pinatubo eruption and this also explains parts of the model discrepancy for the early
16 nineties. Fig. S6 shows that the modeled gradual decline in CO levels over the period 1991-
17 2012 is caused by stable to moderately declining CO emissions over the period combined
18 with increasing OH for most of the period. Much of the large year to year fluctuations in CO
19 levels (black line) are due to variation in emissions (purple line) caused by irregular
20 occurrence and extent of vegetation fires. To summarize, the good agreement between our

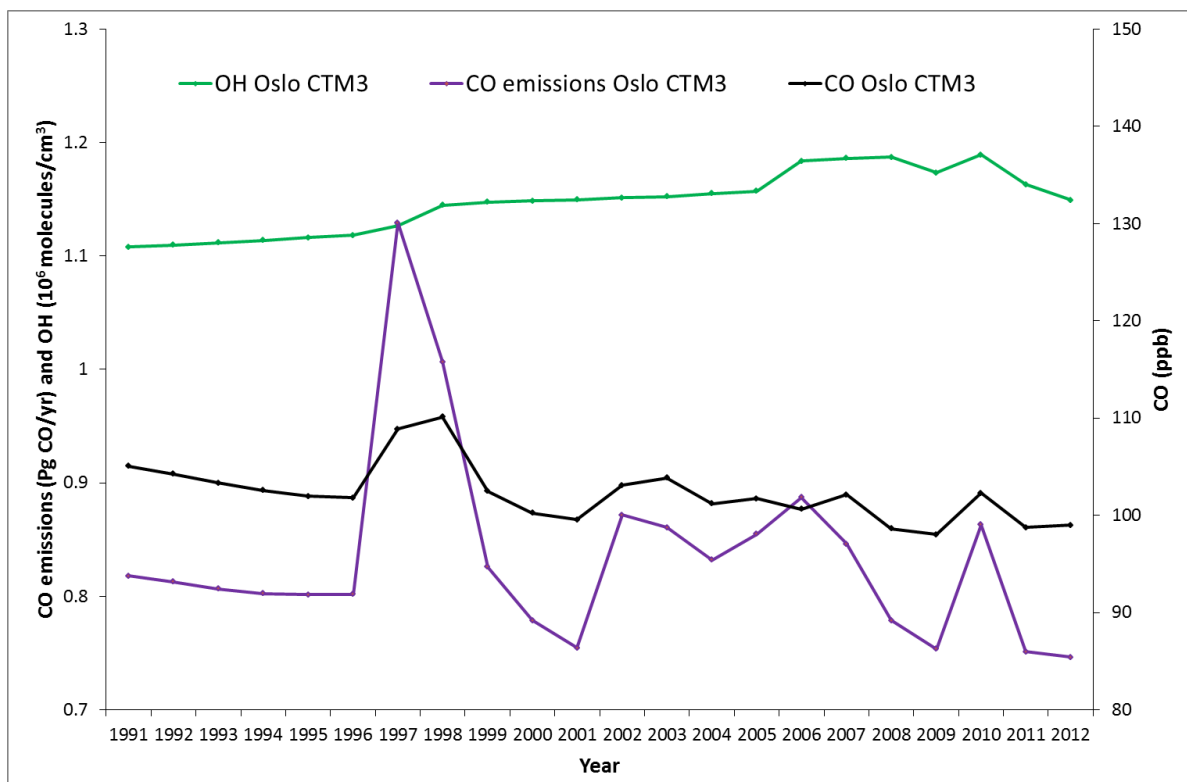
1 model and the observation based estimates supports that the modelled CO, applied CO
2 emission inventory, and calculated OH changes are internally consistent.

3
4 The WDCGG global mean estimate is higher than the NOAA ESRL (Fig. S5) since NOAA
5 ESRL is based on relatively unpolluted marine boundary layer stations while WDCGG
6 include inland stations in their calculations. CO is more unevenly mixed than CH₄ due to its
7 shorter lifetime. How polluted versus un-polluted air masses go in the global mean
8 calculations therefore matters. The modeled global mean is based on all grid-boxes in the
9 lowest model layer and one reason for its higher value might be the above mentioned
10 sensitivity. However, comparing seasonal distributions (not shown) the model seems to
11 overestimate CO levels throughout the Northern Hemisphere summer season and that is likely
12 the main reason for its higher global mean.



14
15 **Figure S5.** Comparison of model and observation based yearly global mean surface CO for
16 the period 1991-2012. NOAA ESRL data set provided by Paul Novelli, personal
17 communication. WDCGG data set (WMO/WDCGG/GAW (2015) provided by WDCGG,
18 personal communication.

19



1
2
3
4
5
6
7
8
9
10
11
12
13
14
15
16
17
18
19
20

Figure S6. Yearly global average atmospheric OH concentration in the main simulation using the reaction rate with CO as averaging kernel and yearly total global CO emissions (left y-axis). Modeled global mean surface CO (right y-axis).

Acknowledgements

We thank WDCGG and Paul Novelli for providing and sharing CO datasets used in figure Figure S5.

References

Bousquet, P., Ringeval, B., Pison, I., Dlugokencky, E. J., Brunke, E. G., Carouge, C., Chevallier, F., Fortems-Cheiney, A., Frankenberg, C., Hauglustaine, D. A., Krummel, P. B., Langenfelds, R. L., Ramonet, M., Schmidt, M., Steele, L. P., Szopa, S., Yver, C., Viovy, N., and Ciais, P.: Source attribution of the changes in atmospheric methane for 2006–2008, *Atmos. Chem. Phys.*, 11, 3689-3700, 10.5194/acp-11-3689-2011, 2011.

Guenther, A., Karl, T., Harley, P., Wiedinmyer, C., Palmer, P. I., and Geron, C.: Estimates of global terrestrial isoprene emissions using MEGAN (Model of Emissions of Gases and Aerosols from Nature), *Atmos. Chem. Phys.*, 6, 3181-3210, 10.5194/acp-6-3181-2006, 2006.

1 Holton, J. R.: An introduction to dynamic meteorology, 3er edition, Academic Press, San
2 Diego, USA, 1992

3 Holtslag, A. A. M., and Boville, B. A.: LOCAL VERSUS NONLOCAL BOUNDARY-
4 LAYER DIFFUSION IN A GLOBAL CLIMATE MODEL, Journal of Climate, 6, 1825-
5 1842, 10.1175/1520-0442(1993)006<1825:lvnbld>2.0.co;2, 1993.

6 Peixoto, J. P., and Oort, A. H.: Physics of climate, Springer-Verlag, New York, USA, 1992.

7 Seinfeld, J. H., and Pandis, S. N.: Atmospheric chemistry and physics: from air pollution to
8 climate change, John Wiley & Sons, New York, USA, 1998

9 Sindelarova, K., Granier, C., Bouarar, I., Guenther, A., Tilmes, S., Stavrakou, T., Müller, J.
10 F., Kuhn, U., Stefani, P., and Knorr, W.: Global dataset of biogenic VOC emissions
11 calculated by the MEGAN model over the last 30 years, Atmos. Chem. Phys. Discuss., 14,
12 10725-10788, 10.5194/acpd-14-10725-2014, 2014.

13 WMO/WDCGG/GAW: Data Summary report, No.39, 2015. Available at
14 <http://ds.data.jma.go.jp/gmd/wdcgg/pub/products/summary/sum39/sum39.pdf>
15